Proceedings of the Institution of Mechanical Engineers, Part J: Journal of Engineering Tribology, Volume 224, Number 1, 2010, pp81-89

The performance of a porous ceramic hydrostatic journal bearing

I S Durazo-Cardenas*, **J Corbett,** and **D J Stephenson**
Cranfield University, Cranfield, Bedfordshire, UK

The manuscript was received on 2 November 2008 and was accepted after revision for publication on 3 April 2009.

DOI: 10.1243/13506501JET570

Abstract: The performance of a porous-ceramic hydrostatic journal bearing manufactured by the starch consolidation (SC) technique has been examined using a highly instrumented test rig. The results have been compared with those of a 5-recess hydrostatic bearing of the same size and comparable design, under the same testing conditions. The SC porous-ceramic bearing showed an improved performance over the conventional hydrostatic bearing. Static and rotational stiffness were 95 per cent and over 150 per cent higher, respectively. In addition, the porous ceramic bearing exhibited a more economic performance with a 64 per cent lower flowrate and pumping power than the hydrostatic bearing. In terms of heat generation, the porous ceramic bearing showed 50 per cent lower temperature rise.

Keywords: porous ceramic, starch consolidation, hydrostatic journal bearing

1 INTRODUCTION

The increasing demand for higher precision and higher speed machining necessitates machine structures and spindle assemblies of higher static and dynamic stiffness than is currently achievable by commercially available machine tools. With the continued drive for improved performance, the limitations of conventional bearing systems have become more evident [**1**]. For example, the medium term accuracy capability of oil hydrostatic bearings is limited by the thermal effects caused by the increased heat generated by viscous shear. Thermal distortion and drift are considered major sources of error in higher precision manufacture [**2**, **3**]. To minimize these effects, an alternative to conventional hydrostatic oil journal bearings has been developed [**4**]. In this technology, the journal bearing is a hollow cylinder made of a porous ceramic material. The externally pressurized lubricant is supplied to the bearing gap through the ceramic bearing's porous wall, as opposed to the 4–6 restrictor/pocket arrangement typically found in conventional hydrostatic bearings. The extremely large number of integrated restrictors, results in an improved fluid film pressure distribution. In addition, the absence of bearing pockets enhances the hydrodynamic component, improving the overall load capacity and stiffness of the bearing [**5**], while permitting the spindle assembly to reach higher speeds before the onset of turbulence.

Other advantages of ceramics as bearing material are low coefficient of expansion, long-term dimensional stability and stiffness over a wide range of temperatures, as well as their superior corrosion resistance. In addition, ceramics can be machined without pore smearing.

Despite all the benefits, porous ceramic hydrostatic journal bearings have yet to be embraced by precision engineers and machine tool designers. So far, the main obstacle has been the intricacy of the bearing's manufacturing method, hot isostatic pressing (HIP). This method consists of the vibration packing of alumina powders followed by partial sintering in a high pressure argon environment [**4**]. Significant machining is required to achieve the ceramic bearing's final dimensions and HIP is a relatively expensive technique. So far, only journal bearings of 50 mm inside diameter and 50 mm long have been achieved, which limits their application. A more recent research effort [**6**] has addressed these issues by investigating alternative processing routes and the development of a processing method that is based on a starch consolidation (SC) technique [**7**]. Cost effective journal bearings of various sizes and porosity levels, suitable for a wide

**Corresponding author: Department of Materials, Cranfield University, Building 70, Cranfield, Bedfordshire MK43 0AL, UK.*
email: i.s.durazocardenas@cranfield.ac.uk

Fig. 1 Porous ceramic hydrostatic journal bearings produced by the SC technique [**6**]

range of precision engineering applications have been produced using this technique (Fig. 1).

In the present study, the bearing performance of a porous ceramic hydrostatic journal bearing produced by the SC technique has been studied. The results are presented in terms of static and rotational stiffness, lubricant flowrate, pumping power and lubricant temperature rise. These results have been compared head to head with the results obtained from a conventional 5-recess hydrostatic journal bearing of the same size and comparable design, under the same testing conditions.

2 EXPERIMENTAL

2.1 Porous ceramic bearing manufacture

The ceramic bearing processing route was the SC technique [**7**]. The SC technique is a simple yet effective method for producing porous ceramics. In simple terms, it involves the mixing of alumina powders, water, starch granules, and a dispersant to create a ceramic slip. The slip is cast into a mould and heated up to 70 °C. At this temperature, the starch granules swell by water uptake and as a consequence, the slip consolidates into a solid body. The starch granules are burnt out in a subsequent de-binding operation, leaving corresponding voids in the ceramic matrix. Further densification at 1550 °C follows. The final porosity of the ceramic bearing is a result of the amount of starch in the slip and the sintering rate of the alumina powder used. Grinding to final dimensions completes the bearing manufacture. Figure 2 illustrates the typical microstructure of a journal bearing produced by the SC technique.

The most important properties and design parameters of the SC porous ceramic bearing tested are shown in Table 1.

2.2 Permeability measurement

The permeability of the porous ceramic bearing was measured using a specially designed test rig compliant with standard BS 5600 [**8**].

Darcy's law describes flow of fluids through porous materials at relatively low velocity, where only viscous factors are prevalent. This equation is used to derive the viscous permeability coefficient (ψ_v) and can be written as follows

$$\frac{\Delta p}{t} = \frac{Q\eta}{A\psi_v} \tag{1}$$

At higher flowrates, inertial effects become significant and Forchheimer's equation [**8**] is used for the determination of the viscous (ψ_v) and inertial permeability (ψ_i) coefficients

$$\frac{\Delta p}{t} = \frac{Q\eta}{A\psi_v} + \frac{Q^2\rho}{A^2\psi_i} \tag{2}$$

Equations (1) and (2) describe the relationship between pressure drop (Δp) and volume flowrate (Q).

During measurement, the journal bearing was clamped axially between two flat sealing surfaces. Pressurized fluid applied from the outside of the bearing permeated inwards through the bearing wall. Ten pressure drop and volume flow readings were taken. The pressure differential across the bearing ranged from 0.1 to 1.0 MPa. The test fluid was oil (DIE 180, BP). Viscosity and density values of 1.9 mm^2/s and 752 kg/m^3 at 20 and 15 °C, respectively, were specified by the lubricant manufacturer. This information was complemented with a more thorough study conducted in accordance with BS 188 [**9**] and 4699 [**10**]. The oil temperature was monitored throughout the measurement to compensate for variations in the density and viscosity values.

Permeability measurement results were predominantly of viscous nature, in agreement with previous work [**4**]. Table 2 illustrates measured Q values against Δp. The calculated viscous permeability of the SC bearing was $2.6 \times 10^{-14}\,m^2$. This was close to the optimum value of $1 \times 10^{-14}\,m^2$ for a porous ceramic journal bearing of the same dimensions, as modelled in a previous study [**4**]. Further details of the permeability measurement procedure can be found elsewhere [**6**, **8**].

2.3 Hydrostatic bearing design and manufacture

The hydrostatic bearing used in this study was of the same size and comparable design to the porous ceramic journal. Well-established guidelines [**11**] were followed for the bearing design and manufacture. Cast iron was used for the construction of the bearing main body and components. A 5-recess/capillary restrictor arrangement was used. The bearing was designed to

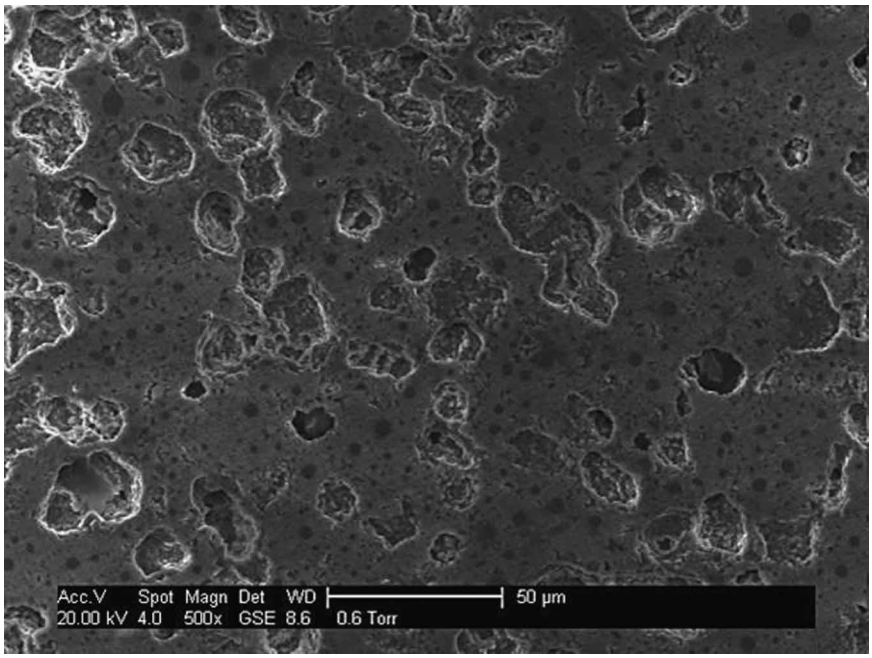

Fig. 2 Microstructure of a porous ceramic journal bearing (present work). Image obtained using a FEI XL30 environmental scanning electron microscope (ESEM)

Table 1 Properties and design parameters of the porous ceramic bearing tested

Journal diameter (m)	Journal length (m)	Wall thickness (m)	Density (g/cm^3)	Permeability (m^2)	Bearing radial gap (μm)	β (dimensionless) [**5**]
0.05	0.05	0.006	2.3	2.6×10^{-14}	26.5	1.74

Table 2 Porous ceramic bearing permeability measurement: pressure drop versus flowrate

Δp (Pa)	Q (m^3/s)
1.00E+05	1.311 85E−06
2.00E+05	5.344 57E−06
3.00E+05	8.239 59E−06
4.00E+05	1.115 82E−05
5.00E+05	1.467 37E−05
6.00E+05	1.750 03E−05
7.00E+05	2.057 31E−05
8.00E+05	2.387 84E−05
9.00E+05	2.751 84E−05
1.00E+06	3.083 42E−05

operate at 4000 r/min. This was an arbitrary value that ensured performance testing was conducted in steady conditions. The bearing was designed to fit in the test rig used for the porous-ceramic bearing testing.

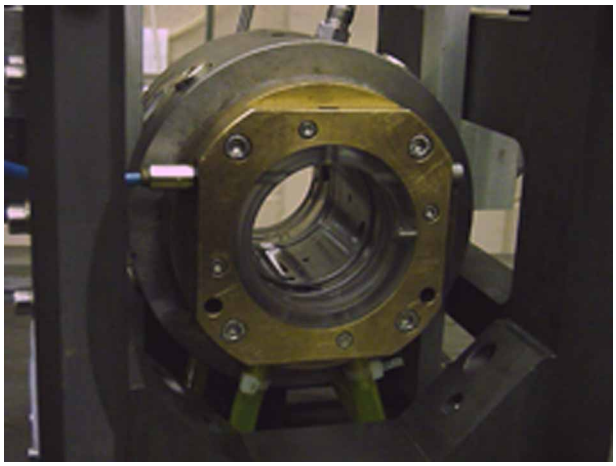

Fig. 3 5-Recess hydrostatic journal bearing

Further details of the bearing dimensions and design parameters can be found in Table 3. Figure 3 shows a photograph of the hydrostatic bearing.

Table 3 Hydrostatic bearing design parameters

Number of pockets	Pocket depth (m)	Resistance ratio (dimensionless)	Restrictor diameter (m)	Circumferential land width (m)	Axial land width (m)	Bearing gap (μm)	Speed (r/min)
5	2.5×10^{-4}	2.2	4.97×10^{-4}	3×10^{-3}	2×10^{-3}	26.5	4000

2.4 Test rig and experimental conditions

Figure 4 illustrates the test rig used. This test rig is a fully instrumented system that includes sensors for measuring the lubricant temperature and pressure at bearing inlet points, within the fluid film, and at the bearing outlet. The test rig houses journal bearings of 50 mm inside diameter, 62 mm outside diameter, and 50 mm long.

The input variables were the supply pressure, bearing speed, and bearing load. A set of four capacitive gauges are used in conjunction with a data acquisition subroutine for the deflection measurement. The capacitive gauges have a specified resolution of 8 nm statically and 40 nm dynamically. Further calibration procedures showed the system was capable of measuring deflection with an overall accuracy of 20 nm statically and 200 nm under rotating conditions [**6**, **12**].

Other ancillary equipments that the testing rig incorporates include a hydrostatic oil power pack, a refrigerated cooling unit, a hydrostatic lubricant power pack with a filter system for total debris and bacterial removal, as well as a comprehensive automated data acquisition system.

Prior to testing, a warm up period of 1 h running at the selected test speed (r/min) was observed. This allowed the conventional oil hydrostatic bearings in the drive spindle to reach a stable operating temperature.

Low viscosity oil (DIE 180, BP) was used as lubricant during the performance testing. This represents a novelty in relation to the performance measurement of porous-ceramic bearings, as only water and air have been used previously [**4**, **13**, **14**]. The oil temperature was monitored to allow corrections of the density and viscosity values where appropriate.

The bearing radial gap for the two types of bearing, porous ceramic and conventional hydrostatic, was 26.5 μm.

Stiffness and flow measurement trials were conducted thrice to verify repeatability. Temperature rise measurements were conducted twice. The maximum error observed was of the order of 5 per cent. Further details of the design and building of this test rig, including operational and calibration procedures have been described extensively before [**4**, **12**].

2.5 Measurement of stiffness

For the measurement of stiffness, the test bearings were positioned in the centre of their working section. A dead weight load was applied using a cable. Stiffness was calculated from the resulting bearing housing deflection with respect to the shaft. Measurements were conducted at a fixed supply pressure of 1.0 MPa. The radial load was gradually incremented from 0 to 100 N in 10 N steps. The results of the static stiffness were plotted against the bearings eccentricity ratio (ε_0). The eccentricity ratio is a porous hydrostatic journal bearing design parameter [**15**], defined by

$$\varepsilon_0 = \frac{e}{C} \tag{3}$$

Rotational stiffness was calculated by measuring deflection under the applied load at different spindle

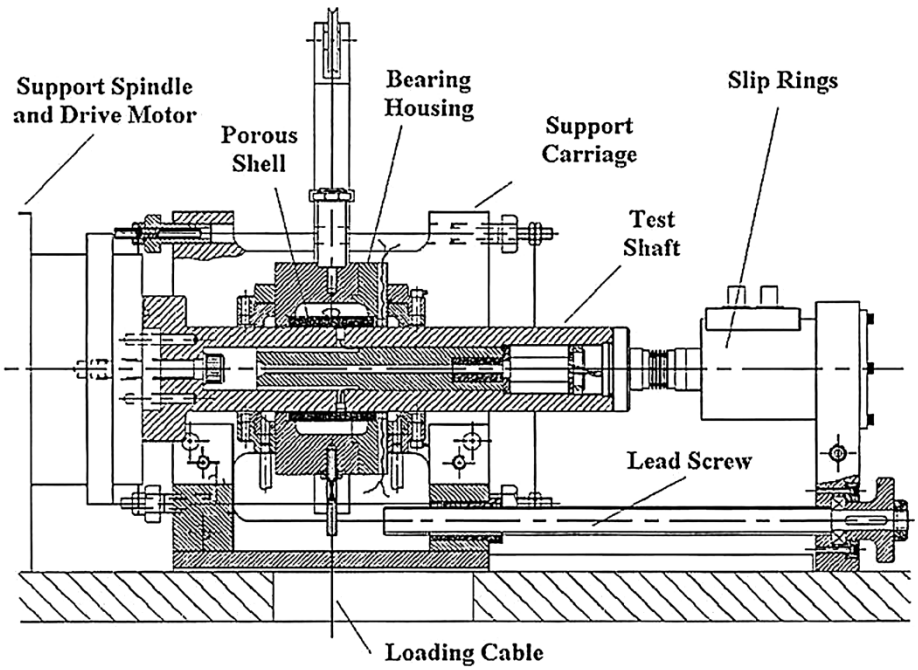

Fig. 4 Porous-ceramic hydrostatic journal bearings performance test rig [**12**]

speeds up to 4000 r/min. Rotational stiffness results are presented in relation to the spindle speed.

2.6 Measurement of flowrate, pumping power, and temperature rise

Flowrate was measured using a weigh tank, a calibrated four-digit resolution digital balance, and a stopwatch. The lubricant inlet and outlet temperatures were also monitored to permit density and viscosity corrections. Flowrate tests were conducted under static conditions, with fixed supply pressures of 0.25, 0.50, 0.75, and 1.0 MPa under no load conditions.

Pumping power was calculated as the product of the lubricant flowrate and the supply pressure.

$$W_{\mathrm{p}} = P_{\mathrm{s}} Q \tag{4}$$

Friction power is dissipated in the bearing fluid film as thermal energy. This causes a corresponding increase in the lubricant temperature. During the temperature rise measurement, the supply pressure was fixed at 1.0 MPa. Previous to the measurement, the spindle was run for 1 h under no load conditions to allow the lubricant's temperature to reach a stable condition. The difference in temperature between bearing's inlet and outlet was then recorded and plotted against the observed spindle speed.

3 RESULTS AND DISCUSSION

3.1 Static stiffness

Figure 5 shows the static stiffness results against the eccentricity ratio for the two bearing types. As seen, the conventional bearing stiffness averaged 22 N/μm, while operating at a supply pressure of 1 MPa. In contrast, the stiffness of the SC bearing was 43 N/μm at the same supply pressure. The higher stiffness observed is attributable to the improved pressure distribution resulting from the multitude of minute restrictors in the porous wall.

The eccentricity ratio values observed for the porous ceramic bearing are quite low in comparison to the hydrostatic bearing, indicating a higher overall bearing stiffness. The observed trend-line is typical of the measurements performed on porous ceramic hydrostatic journal bearings manufactured by the SC technique [**6**]; and, in general, they are also comparable with those observed in previous research [**12**].

3.2 Rotational stiffness results

Figure 6 illustrates the results of the measured rotational stiffness for the porous-ceramic bearing and the conventional 5-recess hydrostatic bearing. Once again, it was observed that the porous-ceramic bearing achieves higher stiffness than the conventional hydrostatic bearing. The stiffness curve of the porous-ceramic bearing displayed a noteworthy growth with the increasing spindle speed. This growth is directly associated with the improved hydrodynamic effect particular to hydrostatic porous bearings, resulting from the absence of bearing pockets. For the porous ceramic bearing tested, this effect is more pronounced after 2000 r/min. At 4000 r/min, the hydrodynamic component of the stiffness was over 80 N/μm, considerably higher than the static stiffness. In contrast, the hydrostatic bearing stiffness displayed a slowly growing curve, demonstrating a less significant hydrodynamic component. At 4000 r/min, the hydrodynamic component of the stiffness was 9 N/μm.

The porous bearing absence of pockets also results in less turbulence. This permitted the stiffness of the porous ceramic bearing to be assessed further. It was observed that the bearing continued to achieve higher stiffness with increasing spindle speeds, reaching a maximum of 167 N/μm at 6000 r/min.

Rotational stiffness results of the porous ceramic bearing are in good agreement with the trends observed in a previous porous ceramic research [**12**].

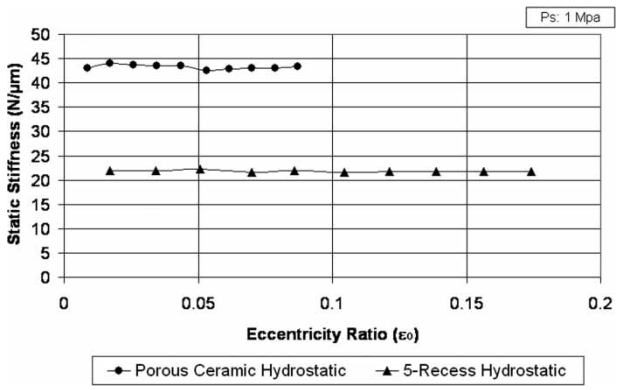

Fig. 5 Bearing technology comparison: static stiffness versus eccentricity ratio

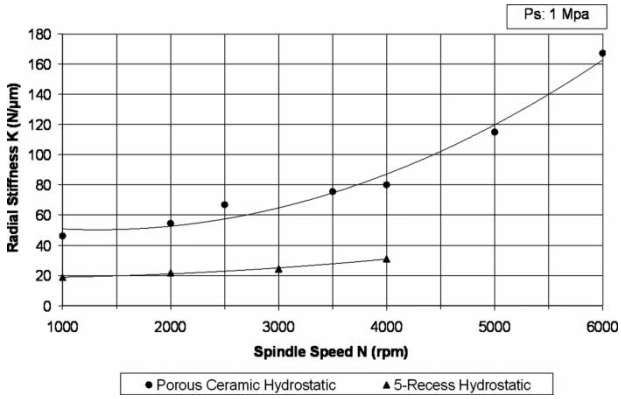

Fig. 6 Bearing technology comparison: rotational stiffness versus spindle speed

3.3 Flowrate measurement results and discussion

Figure 7 illustrates a flowrate comparison between the porous-ceramic bearing and the conventional 5-recess hydrostatic bearing. The flowrate results are presented as a function of the supply pressure. As observed, the conventional hydrostatic bearing flowrate is significantly higher than the porous ceramic bearing. Factors significantly influencing this behaviour are the bearing's radial gap and resistance ratio [**11**]. Conversely, the lower flowrate of the porous bearing resulting from the absence of pockets is mainly influenced by the bearing's permeability [**6**, **12**].

The flowrate characteristics of oil-lubricated porous hydrostatic journal bearings have been studied analytically by Chattopadhyay *et al.* [**5**]. The predicted porous bearing flow is defined by

$$\bar{Q} = \bar{Q}_{\mathrm{c}} + \bar{Q}_{\mathrm{p}} = \frac{Q\eta L}{C^3 D P_{\mathrm{s}}} \tag{5}$$

where

$$\bar{Q}_{\mathrm{c}} = -\frac{1}{6}\int_0^{\theta 2} h^3(1+\zeta_{\mathrm{z}})\left|\frac{\partial \bar{p}}{\partial \bar{z}}\right|_{\bar{z}=1} \mathrm{d}\theta \tag{6}$$

$$\overline{Q_{\mathrm{p}}} = -\left(\frac{\beta}{6}\right)\left(\frac{H}{R}\right)^2 K_{\mathrm{Z}}\int_0^{\theta 2}\int_{-1}^{0}\left|\frac{\partial \bar{p}}{\partial \bar{z}}\right| \mathrm{d}\bar{y}\,\mathrm{d}\theta \tag{7}$$

and

$$\zeta_z = \frac{3(\bar{h}\sigma_z + 2\alpha)}{\sigma_z(\bar{h} + \alpha\overline{\bar{h}^2}\sigma_z)} \tag{8}$$

$$\bar{p} = \left(\frac{p}{P_{\mathrm{s}}}\right) \tag{9}$$

$$\bar{z} = \frac{2z}{L} \tag{10}$$

$$K_z = \left(\frac{k_z}{k_y}\right) \tag{11}$$

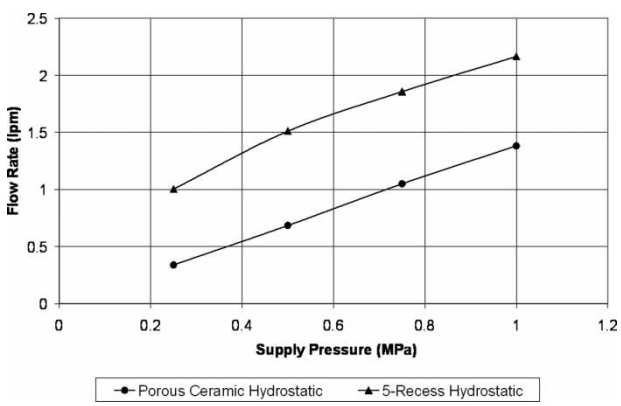

Fig. 7 Bearing technology comparison: flowrate versus supply pressure

$$\bar{y} = \frac{y}{H} \tag{12}$$

$$\bar{h} = \frac{h}{C} \tag{13}$$

$$\sigma_z = C(k_z)^{-1/2} \tag{14}$$

Chattopadhyay [**5**] solved $\bar{Q}$ by numerical integration using Simpson's 1/3rd rule. Flow is presented in terms of dimensionless values of a bearing feed parameter β, the eccentricity ratio ε_0 (equation (3)) and the L/D ratio. The bearing feed parameter is defined by

$$\beta = \frac{12k_y R^2}{C^3 H} \tag{15}$$

For the porous ceramic bearing $\beta = 1.74$.

The experimental data from the porous ceramic bearing have been compared with the predicted flow (equation (5)) using Chattopadhyay's analysis [**5**] and a close correlation has been observed for the different values of P_{s} used. Flowrate results, measured, and predicted, are presented in Table 4.

It was generally observed that the measured flowrate was marginally larger than predicted. This effect was noted previously [**12**], and has been attributed to experimental error arising mainly from a very small amount of lubricant escaping axially through the porous bearing sealing.

3.4 Pumping power

Power consumption is an important parameter when assessing the economic performance of a bearing system. From the flowrates observed, it follows that the pumping power consumed by the conventional hydrostatic is higher. Figure 8 illustrates the calculated pumping power for each bearing in relation to the supply pressure. As observed, the conventional 5-recess hydrostatic bearing consumes more power. The difference in power consumed between the two bearings at a maximum supply pressure of 1.0 MPa was of 13 W.

3.5 Temperature rise

Figure 9 illustrates the temperature increase with spindle speed for the porous ceramic bearing and the

Table 4 Porous ceramic bearing flowrate: measured versus predicted ($\beta = 1.74$)

	Q (m^3/s)	
P_{s} (MPa)	Measured	Predicted [**5**]
0.25	5.65×10^{-06}	5.37×10^{-06}
0.5	1.14×10^{-05}	1.07×10^{-05}
0.75	1.75×10^{-05}	1.61×10^{-05}
1	2.30×10^{-05}	2.15×10^{-05}
1.5	3.46×10^{-05}	3.23×10^{-05}

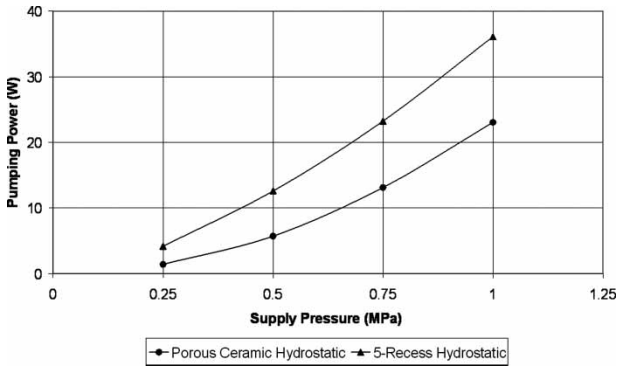

Fig. 8 Bearing technology comparison: pumping power versus supply pressure

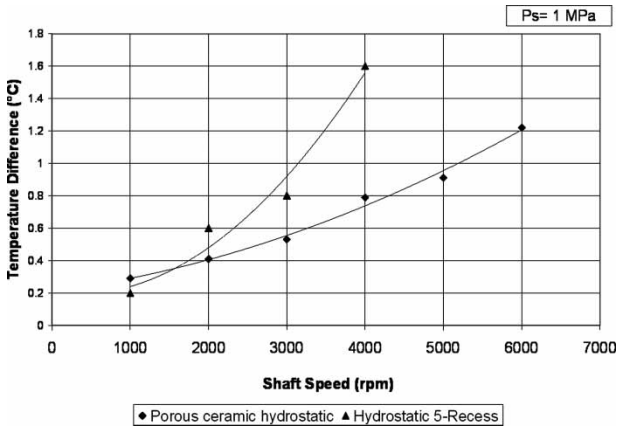

Fig. 9 Bearing technology comparison: temperature rise versus spindle speed

conventional hydrostatic bearing. The higher temperature rise exhibited by the conventional hydrostatic bearing is evident. A maximum temperature difference of 1.6 °C was observed at 4000 r/min. In contrast, the porous-ceramic bearing temperature rise at the same spindle speed was of 0.8 °C. Since the same oil was used as the lubricant in both bearings, the higher temperature exhibited by the conventional hydrostatic bearing is mainly attributable to the effect of re-circulating flow of the lubricant within the bearing pockets, which gives rise to greater frictional drag. This type of flow and its effect is particular to this technology and represents a major drawback for ultra-precision applications. In contrast, in the operation of porous-ceramic hydrostatic bearings, the lubricant readily escapes the bearing gap in a more consistent manner.

4 SUMMARY OF EXPERIMENTAL RESULTS AND DISCUSSION

Table 5 illustrates the results comparing the bearing technologies for each parameter examined. Rotational stiffness and temperature rise tests were conducted at 4000 r/min. The fourth column shows the improvement factor in favour of the porous ceramic bearing.

Table 5 Comparison between a conventional 5-recess hydrostatic bearing and a porous-ceramic bearing. Table shows average values from multiple measurements for each bearing

Performance parameter	Conventional hydrostatic	Porous ceramic	Improvement factor (%)
Static stiffness (N/μm)	22	43	95
Rotational stiffness (N/μm)	31	80	158
Lubricant flowrate (lpm)	2.17	1.38	64
Pumping power (W)	36	23	64
Temperature rise (°C)	1.6	0.8	50

The results observed during the present study illustrate significant benefits of the porous ceramic hydrostatic technology over the conventional one. These results are consistent with a previous analytical performance study comparing a porous ceramic water bearing manufactured via HIP and an oil-lubricated conventional hydrostatic bearing. The stiffness improvement factor in favour of the HIP porous ceramic bearing was of the order of 153 per cent [**12**], which is very similar to the 158 per cent achieved by the SC porous ceramic bearing, as shown in Fig. 6. However, the cost of a porous ceramic journal bearing manufactured by the SC technique is 36 per cent lower than that of a bearing made by the HIP process [**6**].

The lubricant flowrate of porous ceramic was significantly lower than the 5-recess conventional bearing (64 per cent) as expected. This correlated well with a previously published theoretical analysis [**5**]. The porous-bearing lubricant lower viscous-shear resulted in an improvement of 50 per cent on thermal performance compared with the conventional bearing. This porous bearing attributes address directly some of the major sources of error in higher precision manufacture [**2**, **3**].

Hydrostatic journal bearings are a well-established technology. However by virtue of their performance, higher stiffness coupled with lower heat generation and economic performance, porous ceramic hydrostatic journal bearings are a viable alternative to traditional hydrostatic journal bearings for the most demanding high precision applications.

In the past, widespread implementation of porous ceramic technology has been prevented by intricate manufacturing techniques. Recent developments in porous ceramics processing [**6**, **14**] suggest the manufacture of repeatable and cost effective bearings can be successfully achieved.

5 CONCLUSIONS

1. In a head to head performance comparison with a hydrostatic journal bearing of the same dimensions

and comparable design, under identical testing conditions, a porous ceramic demonstrated:
   (a) 95 per cent higher static stiffness, resulting from a more uniform hydrostatic pressure distribution;
   (b) 158 per cent higher rotational stiffness, resulting from an optimized hydrodynamic effect;
   (c) 50 per cent lower lubricant temperature, resulting from a lower lubricant viscous shear;
   (d) 64 per cent lower flowrate, mainly due to the porous bearing having no pocketed recesses;
   (e) 64 per cent lower pumping requirement, resulting from a lower flowrate.
2. Cost effective porous ceramic hydrostatic journal bearings produced by the SC technique exhibit performance characteristics, i.e. stiffness, flowrate, pumping power, and temperature rise that are consistent with the performance of porous ceramic hydrostatic journal bearings produced previously by HIP.

ACKNOWLEDGEMENTS

The authors gratefully acknowledge CONACyT (Mexico) for providing Dr Durazo-Cardenas studentship funds and Mr M. Pierse of Cranfield Precision for his technical assistance and design of the hydrostatic bearing.

REFERENCES

1 **Corbett, J.** Precision machine tools and nanotechnology. In Proceedings of the ESPRC 1st International Conference on Responsive Manufacture, Nottingham, 17–18 September 1997, pp. 143–153.
2 **Slocum, A. H.** *Precision machine design*, 1998 (Prentice Hall, New Jersey).
3 **Weck, M., McKeown, P., Bonse, R.,** and **Herbst, U.** Reduction and compensation of thermal errors in machine tools. *Ann. CIRP*, 1995, **44/2**, 589–598.
4 **Corbett, J., Almond, R. J., Stephenson, D. J.,** and **Kwan, Y. B. P.** Porous ceramic water hydrostatic bearing for improved accuracy performance. *Ann. CIRP*, 1998, **47/1**, 467–470.
5 **Chattopadhyay, A. K.** and **Majumdar, B. C.** Steady state solution of finite hydrostatic porous oil journal bearings with tangential velocity slip. *Tribol. Int.*, 1984, **17/6**, 317–323.
6 **Durazo-Cardenas, I. S.** *Development of porous-ceramic hydrostatic bearings*. PhD Thesis, Cranfield University, Cranfield, UK, 2003.
7 **Lyckfeldt O.** and **Ferreira J. M. F.** Processing of porous ceramic by starch consolidation. *J. Eur. Ceram. Soc.*, 1998, **18**, 131–140.
8 British Standards Institution. Powder metallurgical materials and products part 3. Methods of testing sintered materials – determination of fluid permeability, BS 5600, 1988.
9 British Standards Institution. Methods for the determination of the viscosity of liquids. BS 188, 1977.
10 British Standards Institution. Methods for the determination of the density of petroleum products. BS 4699, 1985.
11 **Stansfield, F. M.** *Hydrostatic bearings*, 1970 (The Machinery Publishing Co. Ltd, Brighton, UK).
12 **Almond, R. J., Corbett, J.,** and **Stephenson, D. J.** Porous ceramic water hydrostatic bearings. In *Total tribology – towards an integrated approach*, 2002, pp. 147–161 (IMechE, London).
13 **Kwan, Y. B. P., Stephenson, D. J.,** and **Alcock, J. R.** The dependence of pore size distribution on porosity in hot isostatically pressed porous alumina. *J. Porous Mater.*, 2001, **8**, 119–127.
14 **Roach C. J.** *Development of porous ceramic air bearings*. PhD Thesis, Cranfield University, Cranfield, UK, 2001.
15 **Majumdar, B. C.** and **Rao, N. S.** On the analytical solution of hydrostatic oil porous journal bearings. In Proceedings of the National Conference on Indian Tribology, 1979, vol. 1, pp. 70–80.

APPENDIX

Notation

A	area of porous material normal to the direction of the fluid flow (m^2)
C	bearing radial clearance (m)
D	bearing diameter (m)
e	eccentricity (μm)
h	local film thickness (m)
$\bar{h}$	dimensionless film thickness
H	thickness of the porous bushing (m)
k_y	viscous permeability coefficient in the y-direction (m^2)
k_z	viscous permeability coefficient in the z-direction (m^2)
K_z	dimensionless permeability in the z-direction
L	bearing length (m)
N	spindle speed (r/min)
p	local film pressure above ambient (Pa)
$\bar{p}$	dimensionless pressure
P_s	lubricant supply pressure (Pa)
Q	lubricant volume flowrate (m^3/s)
$\bar{Q}$	dimensionless flow
$\bar{Q}_c$	dimensionless flow through clearance space
$\bar{Q}_p$	dimensionless flow through porous wall
R	bearing radius (m)
t	thickness of the test piece (m)
W_p	lubricant pumping power (W)
y	radial coordinate (m)
$\bar{y}$	dimensionless radial coordinate
z	axial coordinate (m)
$\bar{z}$	dimensionless axial coordinate
α	slip coefficient

β	dimensionless porous bearing feeding parameter
Δp	pressure drop (Pa)
ε_0	eccentricity ratio (dimensionless)
ζ_z	slip function in the z-direction (dimensionless)
η	lubricant absolute viscosity (Ns/m^2)
θ	dimensionless circumferential coordinate
θ_2	angular extent of un-cavitated film
ρ	density of the test fluid (kg/m^3)
σ_z	dimensionless permeability factor in the z-direction
ψ_i	inertial permeability coefficient (m^2)
ψ_{v}	viscous permeability coefficient (m^2)